Surface Review and Letters, Vol. 20, No. 6 (2013) 1350065 (6 pages)

DOI: 10.1142/S0218625X13500650

PROCESSING–STRUCTURE–PROPERTY CORRELATION IN DC SPUTTERED MOLYBDENUM THIN FILMS

MAJID KHAN[*,¶], MOHAMMAD ISLAM[†,‡,‖], AFTAB AKRAM[‡,**] and UMAIR MANZOOR[§,††]

[*]*National Synchrotron Radiation Laboratory (NSRL)*
and College of Nuclear Science and Technology
CAS Key Laboratory of Soft Matter Chemistry
University of Science and Technology of China (USTC)
Hefei 230029, China

[†]*College of Engineering, King Saud University,*
P. O. Box 800, Riyadh 11421, Saudi Arabia

[‡]*School of Chemical and Materials Engineering,*
National University of Sciences and Technology,
Islamabad 44000, Pakistan

[§]*Department of Physics,*
COMSATS Institute of Information Technology,
Islamabad, Pakistan
[¶]*majids@hotmail.com*
[‖]*miqureshi@ksu.edu.sa*
[**]*aftabakram@scme.nust.edu.pk*
[††]*pakistan@kaist.ac.kr*

Received 12 July 2013
Revised 18 August 2013
Accepted 9 September 2013
Published 5 November 2013

Molybdenum thin films were sputter deposited under different conditions of DC power and chamber pressure. The structure and topography of the films were investigated using AFM, SEM and XRD techniques. Van der Pauw method and tape test were employed to determine electrical resistivity and interfacial strength to the substrate, respectively. All the films are of sub-micron thickness with maximum growth rate of 78 nm/min and crystallite size in the range of 4 to 21 nm. The films produced at high power and low pressure exhibit compressive residual strains, low electrical resistivity and poor adhesion to the glass substrate, whereas the converse is true for films produced at high pressure.

Keywords: Molybdenum; sputtering; PVD; resistivity; strain; films.

[‖]Corresponding author.

1. Introduction

Molybdenum (Mo) coatings or thin films play a key role, both in elemental and compound form, for applications involving tribological and corrosion resistance.[1] Besides structural applications, it can be used as back contact electrode in thin film solar cells.[2–5] Among various metallic films explored as potential back contact layer, Mo and tungsten offer better solar cell efficiencies.[6] Sputter deposited Mo films offer several advantages namely, (i) chemical inertness during deposition of semiconductor absorber layer, (ii) formation of an ohmic contact, (iii) low recombination rate for minority carriers, (iv) stability at processing temperatures, (iv) low contact resistance, and (iv) resistance to alloying with Cu and In, present in the absorber layer. Although Mo films with compressive residual stresses exhibit very low sheet resistance, their adhesion to the underlying glass substrate is very poor. While the films containing tensile stresses adhere well to the substrate, the electrical resistivity increases by an order. Besides adhesion, low electrical resistivity is also important to ensure formation of ohmic contact between the back electrode and the p-type semiconductor absorber layer.

A bilayer configuration with initial film in tension and the subsequent layer under compression is a potential solution that is achievable through careful control of processing parameters. Sputter deposited Mo films with tailored microstructure can also control diffusion of sodium from the glass substrate into the absorber layer.[7] An increase in argon pressure during Mo film deposition causes the amorphous, oxidized phase (MoO_3) intergrain regions to have larger width to act as channels for sodium diffusion intothe absorber layer.[8] It is noteworthy that voids, crystallographic imperfections, and argon or oxygen impurities in Mo films are some of the causes of residual stresses in sputtered thin films. The grain size and the magnitude of tensile stresses have been found to increase with an associated decrease in the surface smoothness in case of heavy inert gas atoms in the plasma discharge.[9]

An important application of Mo thin films is as a back contact electrode in a heterostructure thin film solar cell configuration. In this case, technology scale-up and commercialization perspectives require use of cost-effective and/or flexible substrates, e.g. glass or polyimide sheet, in these solar cells. The key issues to address in this case are interfacial strength and electrical resistivity through intelligent choice of processing parameters. Since any reduction in electrical resistivity occurs at the cost of interfacial strength and vice versa, a compromise needs to be attained for optimum film properties.

In a typical DC-plasma sputtering system, there are several processing parameters; applied power, chamber pressure, gas flow rate and composition (for more than one gases), substrate temperature, target-substrate distance, to name a few.

In this paper, we present work on Mo thin films deposited under different sets of processing conditions. A correlation between the processing conditions and the resulting film structure is established and, in turn, the dependence of film properties (residual stresses, electrical resistivity) on the film structure is elaborated.

2. Experimental Procedure

Using soda-lime glass (SLG) as substrates for Mo film deposition, the cleaning procedure involved ultrasonic cleaning in methanol for 20 min followed by immersion in chromic acid solution for 10 min. After each step, the substrates were cleaned ultrasonically in deionized water for 30 min. Following that, the substrates were blow dried and transferred to the deposition chamber.

Mo thin film deposition was performed using a 3-in Mo target in a magnetron sputtering system (Alliance Concept, DP650) that comprised of mechanical and turbo-molecular pumps, six sputtering guns, DC and RF power supplies, and heating and bias capabilities for substrate support. A typical deposition cycle consisted of the following steps: Evacuation of the chamber to a base pressure of $\leq 10^{-6}$ Torr followed by introduction of argon gas at 2 or 18 sccm (standard cubic centimeter per minute) to achieve desirable chamber pressure; turn on the DC power with its value adjusted to the desirable level; removal of any native oxide layer present on the target surface initially through sputtering of the target with its shutter closed; finally, Mo films of submicron thickness were produced via sputter deposition for certain duration. The applied power of 100 or 200 W corresponds to 2.2 or 4.4 W/cm^2 power densities. The sample identification scheme with processing conditions and some of

Table 1. Sample identification and properties of Mo thin films.

ID	Power (W)	Pressure (mT)	Thickness (nm)	Growth rate (nm/min)	Crystallite size (nm)	Average surface roughness (nm)	Strain (%)	Resistivity ($10^{-6}\Omega$.cm)	Tape test pass/fail
S_1	100	1.5	515	34.3	4.2	1.87	−1.40	202	F
S_2	100	9.2	530	37.9	—	2.16	0.68	257	P
S_3	200	1.5	625	78.1	15.9	2.85	−0.84	42	F
S_4	200	9.2	545	68.1	21.3	1.34	0.56	140	P
S_5	100	3.0	330	36.7	18.2	2.05	−0.04	105	F
S_6	150	3.0	435	54.3	10.0	2.37	2.85	367	P
S_7	200	3.0	680	75.6	—	2.68	3.32	—	F

the properties determined from characterization are listed in Table 1.

Mo film growth morphology and surface microstructure were investigated under scanning electron microscope (SEM) (Model: JSM6460) at 15–20 kV, 30–50 nm spot size and 10 mm working distance. Three-dimensional topography and average surface roughness (R_a) were obtained using atomic force microscope (AFM) (Model: SPM5200) in non-contact mode. The crystallite size and percent strain were determined from X-ray diffractometer (STOE; Stadi MP) with 2θ range, step size, and dwell time values of 36–47°, 0.04° and 3 s, respectively. Residual strain in thin films arises from change in lattice constant with respect to the undeformed lattice (0.3147 nm), and can be expressed as, strain $(\%) = \Delta a/a_o(\%)$. The crystallite size was calculated using Scherrer equation, $t = 0.94\lambda/(\beta \cos\theta)$, where λ, β and θ are wavelength of incident radiation (1.5405 Å for Cu-kα), full-width at half-maximum (FWHM), and diffraction angle, respectively.

Electrical resistivity values were determined through Hall effect measurement system (Ecopia HMS5000). The film adhesion to the substrate was assessed by means of tape test during which an adhesive tape was first applied to the film surface followed by manual removal with approximately the same force. After the test, the sample surface was examined under the optical microscope (Sinowon, UMS-300) to investigate the quality of interfacial adhesion.

3. Results and Discussions

The effect of DC power on film surface and average surface roughness (R_a) was investigated for S_2 and S_4 films, as presented in Fig. 1. The surface microstructure comprises of fine, spherical grains. Although the z values are in the same range, film deposition at 100 W results in formation of isolated islands with more height. Upon increasing the power, the film growth

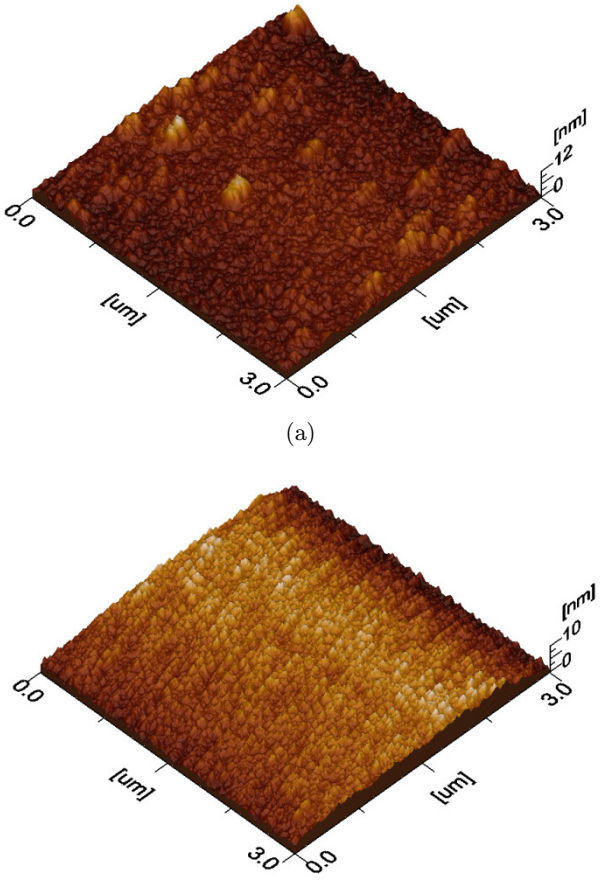

Fig. 1. AFM scans with three-dimensional surface topography for films produced at (a) 100 W (S_2) and (b) 200 W (S_4) (color online).

rate almost doubled from 38 to 68 nm/min, indicating higher sputter yield. Also, surface microstructure is more uniform due to rearrangement and diffusion of the depositing species with enhanced surface mobility. Similar trend has been reported for RF plasma magnetron sputtered nickel, Al_2O_3 and SiO_2 films.[10,11]

An increase in chamber pressure from 1.5 to 3.0 mTorr (S_1 versus S_5) causes a relatively less dramatic increase in deposition rate. As evident from SEM micrographs shown in Fig. 2, the film thickness of sample S_7 (inset of Fig. 2(b)) is uniform (~ 680 nm) over a large substrate area and the surface exhibits very smooth morphology beside appearance of submicron sized features similar to those seen in case of sample S_2 [Fig. 2(a)], presumably due to a drop in energy caused by higher frequency of scattering incidents while in transit from target to the substrate.

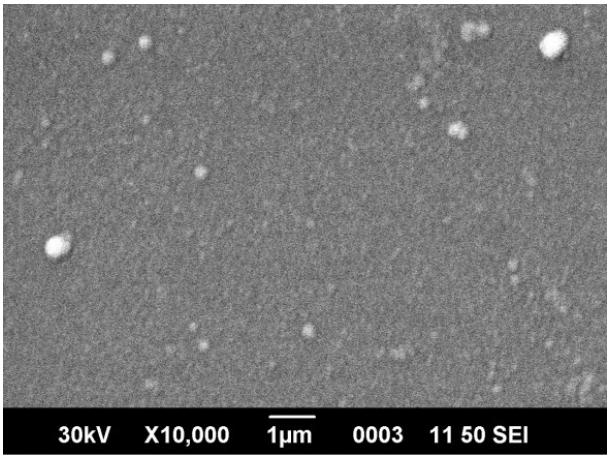

(a)

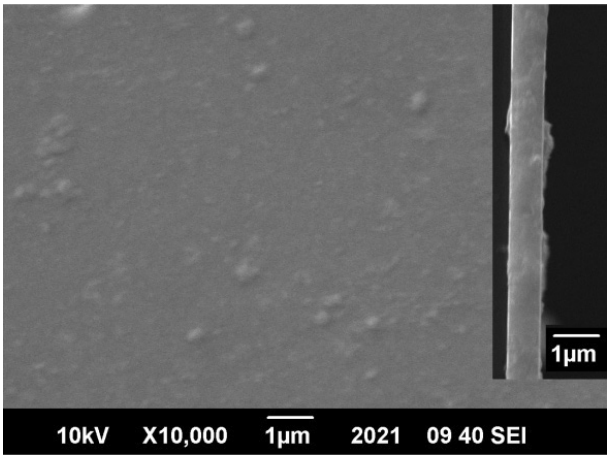

(b)

Fig. 2. SEM microstructures of the S_2 and S_7 films showing microstructure. The inset in (b) is cross-section view of the S_7 film.

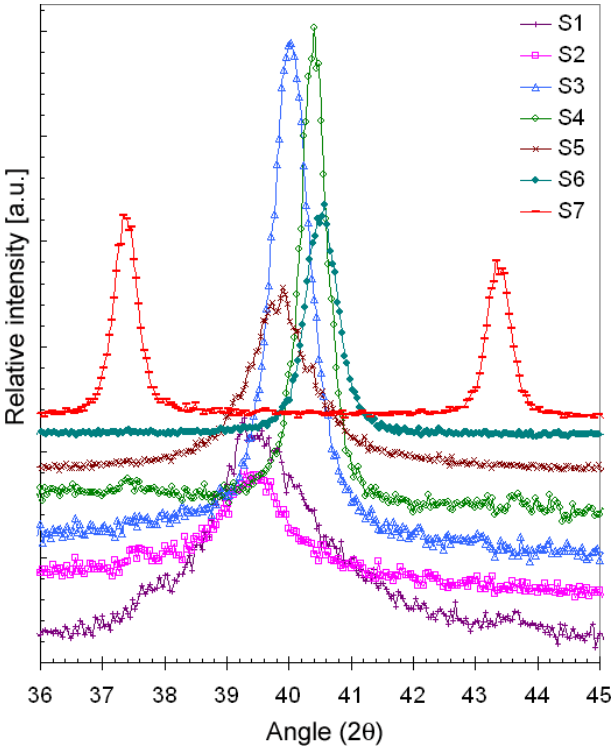

Fig. 3. X-ray diffraction patterns of different Mo films showing precise position of the (110) peak (color online).

X-ray diffraction patterns of the Mo film samples are presented in Fig. 3. Except for the sample S_7, the crystal structure was indexed to be cubic (JCPDS card No. 3-065-7442) with (110) orientation in all cases. The intensity, and in turn, full-width-at-half-maximum (FWHM) value varied for each film. The crystallite size, calculated using Scherrer equation, indicated a general ascending trend with increase in the DC power and/or chamber pressure with values in the range of 4 to 21 nm. The Mo film crystalline quality and crystallite size depend on applied power and chamber pressure through enhanced degree of surface diffusion of the species arriving at the substrate or growing film.[12,13]

The value of residual strain in each film was computed from any shift in (110) peak position with respect to the undeformed crystal lattice. The samples S_1, S_3 and S_5 are noticed to be under compressive stresses with varying magnitudes of corresponding strains. Films deposited at low values of DC power

and pressure exhibit maximum compressive strain due to bombardment of high energy ions in case of sputtering. An increase in pressure causes energy of sputtered species to drop through more scattering events thus inducing porosity in films. For the same DC power of 100 W, an increase in pressure from 1.5 to 3.0 mTorr (S_1 and S_5) caused reduction in compressive strain. Further increase in pressure to 9.2 mTorr changed the nature of residual strain from compressive to tensile. While at low chamber pressure, the sputtered species possess high energy causing strains to develop in the growing film, the mean-free-path of the sputtered species decreases due to higher number of scattering incidents at high pressure with subsequently low stress levels. In general, the magnitude of residual strain is higher at higher power ratings since the sputtering rate increases with an associated increase in the number of energetic particles reaching the surface. Figure 4 presents graphical form of percent strain and electrical resistivity data for all the Mo films. For extreme conditions of power (200 W) and pressure (3.0 mTorr), as in case of sample S_7, the residual strain developed in the film is so high that it causes change of crystal structure from BCC to FCC in order to relieve residual strain. Despite this phase transformation, $\sim 3\%$ strain is still present in the film that compromises on film integrity, causing it to get peeled off.

Investigation into adhesion of Mo films to the SLG substrate through tape test revealed that films deposited at low pressure (1.50 mTorr) such as S_1 fail at the film/substrate interface. On the other hand, Mo film deposited at 9.23 mTorr (e.g. S_4) remain firmly adhered to the substrate. For S_1, S_2 and S_4 films, the surface microstructures examined under optical microscope after tape tests are shown in Fig. 5. The bright regions represent Mo film whereas the dark areas are characteristic of SLG substrate from where the film was delaminated during tape test. The sample S_1 readily failed through film peel-off from most of

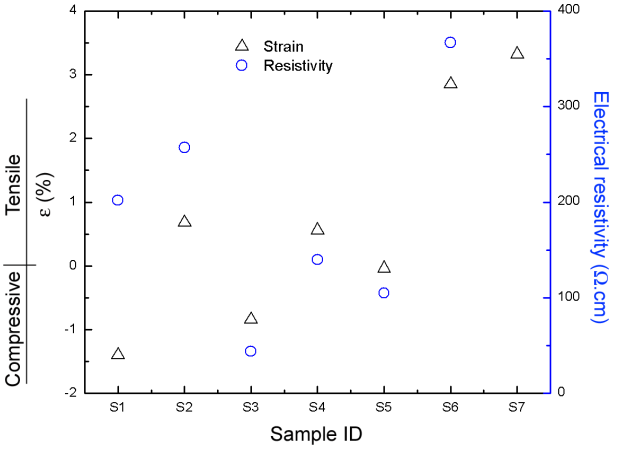

Fig. 4. Graphical representation of residual strain and electrical resistivity data for all the Mo films (Table 1) (color online).

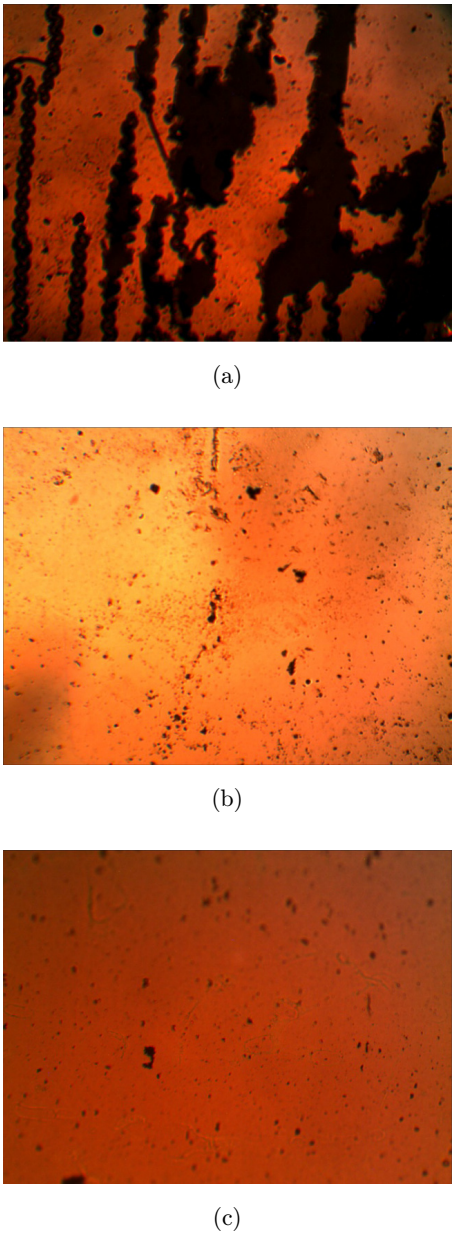

(a)

(b)

(c)

Fig. 5. Optical micrographs of the Mo films (Table 1) after tape test at 400× magnification: (a) S_1, (b) S_2 and (c) S_4 (color online).

the substrate area indicating significantly high magnitude of residual compressive strain. On the other hand, presence of tensile strains as in case of samples S_2 and S_4 did not adversely affect film adhesion since the films retained their structural integrity and remained intact.

The electrical resistivity values for all the films were found to be in the range of 42 to 367 $\mu\Omega$.cm. Samples containing compressive strains exhibit low resistivity values and vice versa. As compared to films produced at 100 W, Mo films prepared at 200 W show low electrical resistivity. Film deposition at high chamber pressure induces porosity into growing films with columnar growth morphology and an associated increase in resistivity.[14] The minimum electrical resistivity is higher by almost an order than that of its bulk value (5.4 $\mu\Omega$.cm). For all the films, the resistivity data is plotted in Fig. 4. Low electrical resistivity values are desirable in order to minimize contribution of Mo back contact layer to the solar cell's series resistance. A post-deposition annealing treatment at temperatures can improve film hardness beside other potential advantages of sodium diffusion from SLG and MoSe formation at the Mo/CIGSe interface.

4. Conclusion

In this paper, we present Mo thin film deposition at different values of DC power and chamber pressure. Microstructural examination confirms nanocrystalline nature of the sub-micron thick films as determined using Scherrer equation. The films exhibit presence of compressive or tensile residual strains depending on the combination of power and pressure. Film growth at high power and low pressure can even cause phase transformation from BCC to FCC crystal structure. The electrical resistivity of the films can be minimized through formation of dense structure as a result of less scattering incidents and diffusion during growth. The adhesion improves when the nature of residual strains is tensile. Sputtered Mo thin films with adequate adhesion and minimum electrical resistivity can be used for solar cell and other microelectronics applications.

Acknowledgements

The authors would like to extend their sincere appreciation to the Deanship of Scientific Research at King Saud University for its funding of this research through the Research Group Project no. RGP-VPP-283.

References

1. G. Jin, B.-S. Xu, H.-D. Wang, Q.-F. Li and S.-C. Wei, *Surf. Coat. Technol.* **201**(15) (2007) 6678.
2. Z. H. Li, E. S. Cho and S. J. Kwon, *Appl. Surf. Sci.* **257** (2011) 9682.
3. F. Dejene, *J. Mater. Sci.* **46**(21) (2011) 6981.
4. T. K. Todorov, K. B. Reuter and D. B. Mitzi, *Adv. Mater.* **22** (2010) E156.
5. H. Katagiri, K. Jimbo, S. Yamada, T. Kamimura, W. S. Maw, T. Fukano, T. Ito and T. Motohiro, *Appl. Phys. Exp.* **1** (2008) 041201.
6. K. Orgassa, H. W. Schock and J. H. Werner, *Thin Solid Films* **431**–**432** (2003) 387.
7. H. A. Al-Thani, F. S. Hasoon, M. Young, S. Asher, J. L. Alleman, M. M. Al-Jassim and D. L. Williamson, *29th IEEE PV Specialists Conf.*, New Orleans, Louisiana (2002).
8. E. Gautron, M. Tomassini, L. Arzel and N. Barreau, *Surf. Coat. Technol.* **211** (2012) 29.
9. G. T. West and P. J. Kelly, *Surf. Coat. Technol.* **206** (2011) 1648.
10. M. Islam, O. T. Inal and J. R. Luke, *J. App. Phys.* **100** (2006) 084903.
11. M. Islam and O. T. Inal, *J. Vac. Sci. Technol. A* **26**(2) (2008) 198.
12. L. Assmann, J. C. Bernede, A. Drici, C. Amory, E. Halgand and M. Morsli, *Appl. Surf. Sci.* **246** (2005) 159.
13. Y. W. Yen, Y. L. Kuo, J. Y. Chen, C. Lee and C. Y. Lee, *Thin Solid Films* **515** (2007) 7209.
14. S.-Y. Kuo, L.-B. Chang, M.-J. Jeng, W.-T. Lin, Y.-T. Lu and S.-C. Hu, *Res. Soc. Symp. Proc.* **1123** (2009) P05–18.